JBC EDITORS' PICK

AC6 regulates the microtubule-depolymerizing kinesin KIF19A to control ciliary length in mammals

Received for publication, April 18, 2020, and in revised form, July 9, 2020 Published, Papers in Press, July 18, 2020, DOI 10.1074/jbc.RA120.013703

Kavisha Arora[1], **John R. Lund**[1], **Nevin A. Naren**[1], **Basilia Zingarelli**[2], **and Anjaparavanda P. Naren**[1,*]

From the Divisions of [1]*Pulmonary Medicine and* [2]*Critical Care Medicine, Department of Pediatrics, Cincinnati Children's Hospital Medical Center, Cincinnati, Ohio, USA*

Edited by Enrique M. De La Cruz

Motile cilia are hairlike structures that line the respiratory and reproductive tracts and the middle ear and generate fluid flow in these organs via synchronized beating. Cilium growth is a highly regulated process that is assumed to be important for flow generation. Recently, Kif19a, a kinesin residing at the cilia tip, was identified to be essential for ciliary length control through its microtubule depolymerization function. However, there is a lack of information on the nature of proteins and the integrated signaling mechanism regulating growth of motile cilia. Here, we report that adenylate cyclase 6 (AC6), a highly abundant AC isoform in airway epithelial cells, inhibits degradation of Kif19a by inhibiting autophagy, a cellular recycling mechanism for damaged proteins and organelles. Using epithelium-specific knockout mice of AC6, we demonstrated that AC6 knockout airway epithelial cells have longer cilia compared with the WT cells because of decreased Kif19a protein levels in the cilia. We demonstrated *in vitro* that AC6 inhibits AMP-activated kinase (AMPK), an important modulator of cellular energy-conserving mechanisms, and uncouples its binding with ciliary kinesin Kif19a. In the absence of AC6, activation of AMPK mobilizes Kif19a into autophagosomes for degradation in airway epithelial cells. Lower Kif19a levels upon pharmacological activation of AMPK in airway epithelial cells correlated with elongated cilia and vice versa. In all, the AC6–AMPK pathway, which is tunable to cellular cues, could potentially serve as one of the crucial ciliary growth checkpoints and could be channeled to develop therapeutic interventions for cilia-associated disorders.

Motile cilia are numerously present moving structures that are crucial for flow generation in the airway epithelium, brain ventricle, oviducts, and middle ear. Defects in formation, maintenance, and function of motile cilia can result in ciliopathies that usually manifest as multisystem problems (1, 2). Ciliary length adjustment is an important parameter for control of cilia-generated fluid flow; however, the mechanisms that optimize this process remain less defined. It is argued that cilia length is crucial to precisely define cilia and mucus contact (~10%) that affects ciliary forward and backward strokes (3). Stress caused by smoking, pathogen infection, and air-borne toxins depress mucociliary clearance, a process of airway cleansing that has been associated with altered cilia length (4, 5). A kinesin 8 motor protein, Kif19a, was reported to be a key determinant of optimal ciliary length through its microtubule-depolymerizing activity at the ciliary tips (6). Consistently, loss of Kif19a leads to elongated cilia, improper cilia-generated flow, and ciliopathies in *Kif19a*$^{-/-}$ mice.

Cilia are not merely microtubular structures but form highly specialized signaling compartments enriched with cellular messengers including cAMP and Ca^{2+} (7). Adenylate cyclases 5 and 6 (AC5/6) are the major suppliers of cAMP in nonmotile cilia (7, 8). Primary cilium length is known to be sensitive to intracellular cAMP dependent upon AC5/6 activity (9). In the context of motile cilia, the role of cAMP is known to be as an important regulator of ciliary beating and organization of compartmental signaling (10, 11). Whether ACs and cAMP regulate motile cilia growth and development has not been explored before. Also, the dynamic and reversible nature of motile cilia length remain unrecognized. More recently, the role of autophagy has been redefined to selectively clear primary cilia-associated proteins in autophagosomes fused with lysosomes that control ciliogenesis and ciliary growth (12, 13). This prompted our interest in investigating whether Kif19a is an autophagy substrate that may become relevant to motile cilia growth. Autophagy can become triggered by activation of AMPK, a heterotrimeric complex of a catalytic (α) and regulatory (β and γ) subunits, because it stimulates mechanisms to conserve energy and resources (14, 15). Active AMPK (Thr(P)^{172}–AMPK) stimulates autophagy indirectly via negative regulation of mTORC1 kinase complex and can directly activate it through directly binding, phosphorylating, and activating autophagy-initiating kinase Ulk1 (16). Protein kinase A also negatively regulates autophagy by impeding AMPK–Thr^{172} activation through phosphorylation at Ser^{173} and hampering ULK1 activation (17). In this study, we identified that AC6 activity inhibits AMPK activity and controls Kif19a protein levels via regulation of autophagy to alter motile cilia length and function, which can be mimicked by pharmacologically targeting of the AMPK pathway. Our study identified an important signaling pathway that can be directly targeted to alter motile cilia length of potential relevance to cilia-associated disorders.

Results

AC6 knockout mice have longer and functionally impaired cilia in the airway epithelium

Based on RNA-sequencing data in primary human bronchial epithelial cells (PHBECs) and mouse trachea, AC6 emerged as the predominant AC isoform (Fig. 1*A*). Using a sonic hedgehog cre (Shh cre) driver, we generated epithelial knockout of AC6

This article contains supporting information.

* For correspondence: Anjaparavanda P. Naren, anaren@cchmc.org.

and confirmed reduced AC protein expression using AC5/6 antibody in isolated *Adcy6*$^{f/f\ Shh\ Cre/+}$ (*Adcy6*$^{\Delta/\Delta}$) mice tracheal epithelial cells (Fig. 1*B*). Considering a known role of cAMP in mucociliary clearance, we tested cilia-generated flow in *Adcy6*$^{\Delta/\Delta}$ mice and observed a 2.4-fold lower particle movement in *Adcy6*$^{\Delta/\Delta}$ compared with *Adcy6*$^{\Delta/\Delta}$ mice trachea (Fig. 1, *C* and *D*, and Movie S1). Based on this observation, we considered the possibility of cilia-associated defects in *Adcy6*$^{\Delta/\Delta}$ mice. Immunostaining data revealed apical enrichment of AC6 in the large airways (trachea) and localization not along the cilia but rather with the ciliary basal body marker γ-tubulin (Fig. 1, *E* and *F*). Based on our experimental determination, we hypothesized that defective ciliary movement in *Adcy6*$^{\Delta/\Delta}$ tracheal epithelial cells could be in part due to longer cilia compared with the control mice (30% longer; 3.9 ± 0.7 in *Adcy6*$^{f/f}$ *versus* 5.1 ± 0.7 in *Adcy6*$^{\Delta/\Delta}$) (Fig. 1, *G* and *H*). We were able to recapitulate these findings using PHBECs. We measured the length of ciliary tuft and isolated cilia and observed an ∼50% increase in the cilia length upon lentiviral knockdown of AC6 expression using two separate shRNAs (Fig. 1, *I* and *J*). Based on these findings, we can conclude a prominent mucociliary clearance defect and elongated cilia upon loss of AC6 in the airway epithelium.

AC6 knockout mice cilia are deficient in Kif19a

Niwa *et al.* (6) identified Kif19a as a ciliary tip protein that acts as microtubule depolymerizing kinesin at the distal end of the cilia to regulate length. We observed that Kif19a was enriched at the ciliary tips and colocalized with ciliary tip marker EB1 but also expressed along the length of the cilium (Fig. 2*A*). We observed that lentiviral knockdown of Kif19a significantly increased ciliary length by >2-fold in PHBECs and mouse tracheal epithelial cells (MTECs) grown on the Transwells (Fig. 2, *B–D*). Therefore, we were able to confirm that Kif19a is a direct negative regulator of ciliary length as demonstrated previously (6). Based on our earlier observation of longer cilia in *Adcy6*$^{\Delta/\Delta}$ tracheal cells, we proceeded to investigate whether Kif19a is a possible target of AC6 in controlling ciliary length. Interestingly, Kif19a protein levels were dramatically reduced in *Adcy6*$^{\Delta/\Delta}$ trachea compared with the control, which was not at the level of transcripts (Fig. 2, *E* and *F* and Fig. S1*A*). Consistent with the observations above, transient overexpression of AC6 increased His-S-Kif19a (isoform 2, ∼70 kDa) levels by 2-fold that did not concur with the possibility of reduced proteosomal degradation (Fig. 2, *G* and *H*, and Fig. S1*B*). Until this point, we can conclude that down-regulation of AC6 expression phenocopies loss of Kif19a.

Kif19a is an autophagy substrate

We next asked how AC6 affects Kif19a protein levels. Given the recently established role of autophagy in ciliogenesis (10, 11) and the interconnected AMPK–autophagy pathways, we proceeded to test whether the components of autophagy and AMPK pathway are altered in *Adcy6*$^{\Delta/\Delta}$ epithelial cells. Indeed, up-regulated AMPK signaling, for example, increased P-AMPK-α–Thr^{172} and down-regulation of P-mTOR were observed in *Adcy6*$^{\Delta/\Delta}$ isolated MTECs relative to the control (Fig. 3, *A* and *B*). Also, autophagy was up-regulated in *Adcy6*$^{\Delta/\Delta}$ tracheal cells as indicated by increased lipidation of LC3 (LC3-II), an autophagy marker (Fig. 3, *A* and *B*). Next, we tested the possibility that AMPK-mediated autophagy might regulate Kif19a expression in *Adcy6*$^{\Delta/\Delta}$ epithelial cells. First, we identified an interaction between Kif19a and the endogenous and overexpressed P-AMPK-α subunit (Fig. 3, *C* and *D*, and Fig. S2). Second, coexpression of recombinant AC6 compromised an interaction of Kif19a with AMPK-α (Fig. 3, *C* and *D*). Also, lowered P-AMPK-α and in the presence of AC6 overexpression suggested that AC6 impedes AMPK activation as corroborated by our findings in Fig. 3 (*A* and *B*). Importantly, we concluded that Kif19a preferentially interacts with the P-AMPK or active AMPK as Kif19a interaction with total AMPK followed an interaction pattern of P-AMPK (Fig. 3, *C* and *D*). Next, we investigated how modulation of AMPK activity may affect Kif19a protein levels. Treatment of cells with the inhibitor of AMPK activity, compound C enhanced while AMPK activator-AICAR decreased, Kif19a protein expression without altering the total levels of acetyl-CoA carboxylase, a direct AMPK target (Fig. 3, *E* and *I*). To investigate whether Kif19a is cleared in the autophagosomes because of an increased autophagy in AC6 KO tracheal cells, we tested Kif19a protein levels in cells treated with pharmacological activators (Torin1) and inhibitors (chloroquine (CQ)) of autophagy and in cells deficient for autophagy (generated upon knockdown of ATG5 expression) (Fig. 3, *E–I*). The incubation of cells with Torin1 decreased Kif19a protein expression in a dose-dependent manner, and Kif19a protein expression was increased in cells treated with both CQ and ATG5 sh (Fig. 3, *E–I*). To test whether AMPK drives Kif19a recruitment into autophagosomes, we performed *in vitro* colocalization study between Kif19a and LC3 in MTECs. An extensive accumulation of Kif19a was observed in LC3-positive autophagosomes in *Adcy6*$^{\Delta/\Delta}$ MTECs that was marginal in *Adcy6*$^{f/f}$ MTECs (Fig. 3, *J* and *K*). Inhibition of AMPK activity stalled Kif19a localization into autophagosomes in *Adcy6*$^{f/f}$ and *Adcy6*$^{\Delta/\Delta}$ MTECs, whereas AMPK activation enhanced this process in *Adcy6*$^{f/f}$ MTECs (Fig. 3, *J* and *K*). In summary, AC6 down-regulates AMPK activation and prevents P-AMPK-Kif19a protein interaction, and AMPK activation drives Kif19a recruitment into autophagosomes for clearance.

Loss of AMPK restores ciliary length in AC6 knockout mice

Next, we investigated how the above described mechanism might translate into ciliary length regulation. Ciliary length negatively correlated with the endogenous Kif19a expression (determined using immunofluorescence) in MTEC cilia (Fig. 4*A*). Inhibition of AMPK reversed longer cilia in *Adcy6*$^{\Delta/\Delta}$ MTECs that correlated with increased Kif19a expression (Fig. 4*B*). Treatment of tracheal cells with AICAR significantly increased the length of *Adcy6*$^{f/f}$ cilia correlating with decreased Kif19a expression (Fig. 4*B*). This effect of AICAR was blunted in *Adcy6*$^{\Delta/\Delta}$ cilia, suggesting that the activation of AMPK pathway in *Adcy6*$^{\Delta/\Delta}$ tracheal cells may already be saturated, and also, no apparent change in Kif19a expression was observed under these conditions (Fig. 4*B*). These findings suggest that loss of Kif19a expression coincides with abnormal elongation

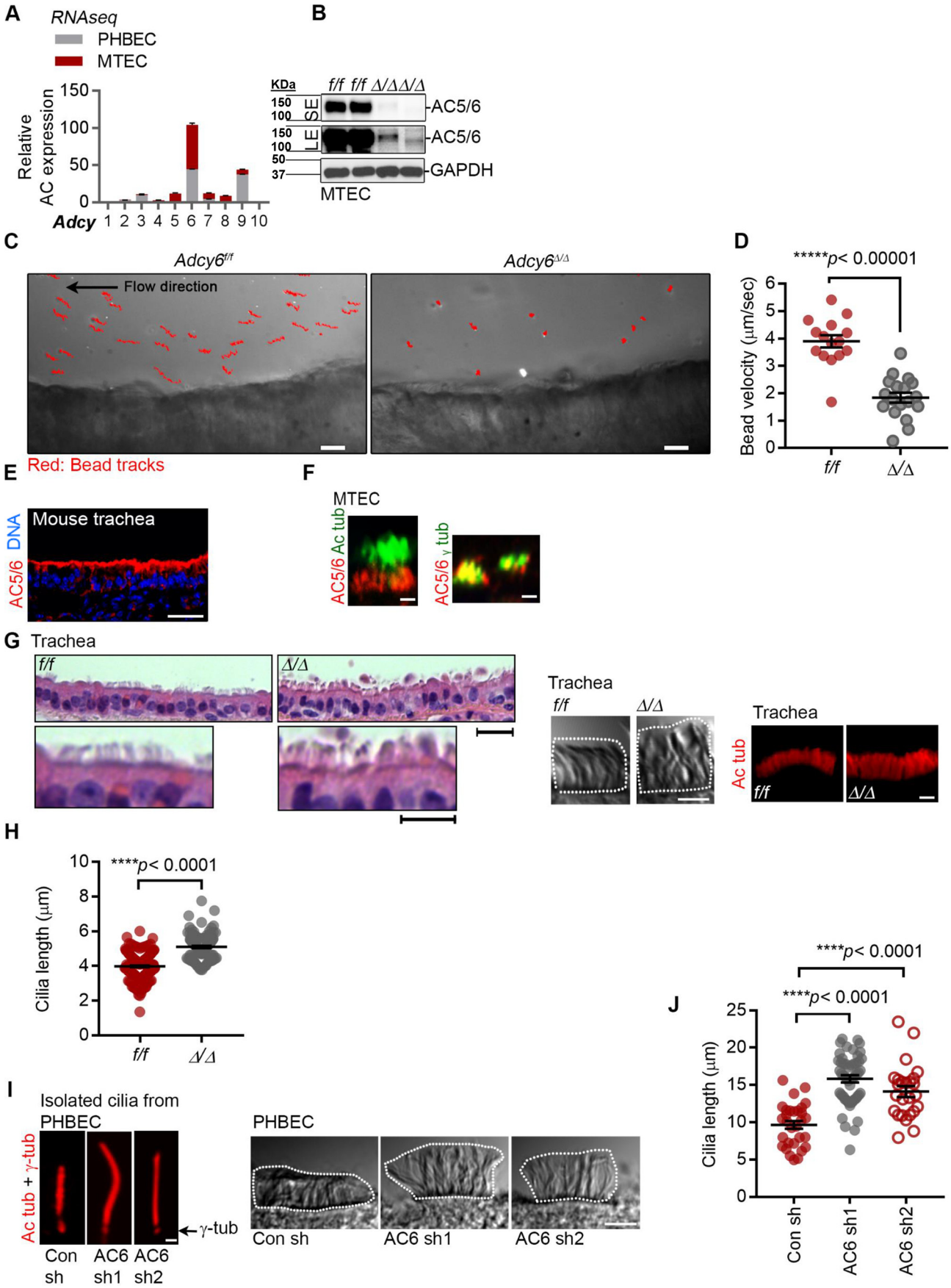
A
RNAseq
PHBEC
MTEC
Relative AC expression
Adcy 1 2 3 4 5 6 7 8 9 10
B
KDa
f/f f/f Δ/ΔΔ/Δ
SE
LE
AC5/6
AC5/6
GAPDH
MTEC
C
Adcy6f/f
Adcy6Δ/Δ
Flow direction
Red: Bead tracks
D
*****p< 0.00001
Bead velocity (μm/sec)
f/f
Δ/Δ
E
Mouse trachea
DNA
AC5/6
F
MTEC
AC5/6 Ac tub
AC5/6 γ tub
G
Trachea
f/f
Δ/Δ
Trachea
f/f
Δ/Δ
Trachea
Ac tub
f/f
Δ/Δ
H
****p< 0.0001
Cilia length (μm)
f/f
Δ/Δ
I
Isolated cilia from PHBEC
Ac tub + γ-tub
γ-tub
Con sh
AC6 sh1
AC6 sh2
PHBEC
Con sh
AC6 sh1
AC6 sh2
J
****p< 0.0001
****p< 0.0001
Cilia length (μm)
Con sh
AC6 sh1
AC6 sh2

of $Adcy6^{\Delta/\Delta}$ cilia. Also, the AC6 and AMPK pathways cooperatively act to regulate motile cilia length. The abnormally long cilia measured in $Adcy6^{\Delta/\Delta}$ *ex vivo* trachea correlated with poor cilia-generated flow (Fig. 4*C*). Treatment of $Adcy6^{\Delta/\Delta}$ tracheal samples with Comp. C (4 h) improved cilia-elicited bead velocity that correlated with shorter cilia length. Treatment of $Adcy6^{f/f}$ tracheal samples with AICAR (4 h) impaired cilia-generated flow correlating with longer cilia (Fig. 4*C*). Hence, there is a clear negative correlation between longer cilia height and impaired cilia-generated flow. Overall, these findings imply that the abnormal cilia-generated flow in $Adcy6^{\Delta/\Delta}$ airways can be at least explained by longer than normal cilia in these mice.

Discussion

Overall, we present a previously unidentified mechanism of dynamic regulation of motile cilia length (Fig. 4*D*). Previous study showed that there is a dose dependence of Kif19a to cilia length (6). Because Kif19a is a plus-end-directed motor, plus-end being the growing distal end of cilia, Niwa *et al.* (6) suggested that this means a more efficient way to regulate ciliary length compared with both plus- and minus-end-directed microtubule rearrangement (6). Based on the marked ciliary phenotype in $Kif19a^{-/-}$ mice as reported earlier, it is very unlikely that there is a redundancy to the role of Kif19a, and it seems to be conserved. This makes Kif19a a key determinant of the optimal length of motile cilia in mammals. It is suggested that Kif19a depolymerizes microtubules in a length-dependent manner that is important for the dynamic aspect of ciliary growth (18).

Autophagosomes carry highly selective protein cargos for degradation that becomes crucial to the homeostatic balance of the cell. Several of these cargos are recruited based on their interaction with the specific components of the autophagic machinery, and in this manner, autophagy can be a selective pathway. LC3-II, a specific autophagy marker, serves as the membrane receptor to select and recruit cargoes for lysosomal degradation. Autophagy has recently been shown to function in the growth of primary cilia (13). LC3 has been demonstrated to interact with a group of centriolar satellite proteins, including PCM1, CEP131, and OFD1 (19). OFD1 is removed from centriolar satellites upon serum starvation at the initiation of ciliogenesis via autophagy. The relationship between ciliogenesis and autophagy could be more complex because autophagy also appears to limit ciliogenesis by eliminating Ift20, an essential component of ciliary transport (13). These distinct roles of autophagy in ciliogenesis could be related to the type of ciliogenesis, *i.e.* basal *versus* induced (*e.g.* by starvation) (13). Furthermore, HDAC6 regulates autophagy during autophagosome–lysosome fusion to mediate autophagy-mediated cilia disassembly via degradation of ciliary protein IFT88 (20). In this study, HDAC6 was shown to be a critical regulator of autophagy-mediated cilia shortening caused by cigarette smoke exposure and as a potential therapeutic target for COPD (20). Although testing the interaction of Kif19a with the core autophagy proteins is pending, we identified that Kif19a interacts with AMPK, an important upstream regulator of autophagy, suggesting it to be a selective pathway involving autophagy. Inhibition of AMPK perturbed Kif19a-LC3 localization; however, LC3-labeled autophagosomes were distributed in close proximity to Kif19a protein clusters. This suggests that autophagosomes closely guard and calibrate Kif19a levels to render ciliary length alteration very sensitive to cellular changes. The fact that longer cilia in $Adcy6^{\Delta/\Delta}$ airways beat slower could suggest that this is an energy-conserving mechanism employed by cells and made into effect by up-regulated AMPK–autophagy pathway.

Our findings identified key molecular factors that cooperatively regulate Kif19a levels to mediate ciliary length control in mammals. This study provides an important piece of evidence to support inherent plasticity in motile cilia that may be crucial during key developmental events and in adult mammalian function.

Experimental procedures

Mice

$Adcy6^{f/wt}$ mice were obtained from The Jackson Laboratory following cryorecovery and were interbred to obtain $Adcy6^{f/f}$ mice. $Adcy6^{f/f}$ mice were then crossed with Shh GFP cre mice (B6.Cg-$Shh^{tm1(EGFP/cre)Cjt}$/J, The Jackson Laboratory); following a series of intercrosses, $Adcy6^{\Delta/\Delta}$ mice ($Adcy6^{f/f}$ $Shh^{tm1(EGFP/cre)/wt}$ mice) were obtained. The male mice were used as Shh GFP cre donors. As a control to $Adcy6^{\Delta/\Delta}$ mice, littermate $Adcy6^{f/f}$ mice were used. Typically, 6–12-week-old male mice were used for the study. All the mice were maintained in a barrier facility at Cincinnati Children's Hospital Medical Center and were fed normal chow. All procedures were performed in compliance with institutional guidelines and were approved

Figure 1. AC6 KO airway cilia have abnormal length and function. *A*, RNA-sequencing analysis demonstrated a relative abundance of transcripts of adenylate cyclases 1–10 in PHBECs ($n = 4$) and MTECs ($n = 3$). AC6 and AC9 were found to be the most abundant ACs in human bronchial cells, and AC6 emerged as the most dominant AC isoform in the murine trachea. *B*, Western blotting was probed using AC5/6 antibody to confirm the loss of AC6 expression in $Adcy6^{\Delta/\Delta}$ tracheal epithelial cells. GAPDH was used as a loading control. *SE* and LE refer to short and long exposures of the film, respectively. *C*, bead flow assay to determine cilia-generated fluid flow plotted from Movie S1 in $Adcy6^{f/f}$ and $Adcy6^{\Delta/\Delta}$ tracheal rings (*scale bar*, 10 μm). Trajectories followed by the beads are represented in *red*. *D*, quantitation of bead velocity in $Adcy6^{f/f}$ and $Adcy6^{\Delta/\Delta}$ mouse trachea ($n = 5$ mice per group, three regions per tracheal ring). Each *dot* represents a region. *E* and *F*, confocal images demonstrating AC5/6 immunostaining in mouse trachea isolated from $Adcy6^{f/f}$ and $Adcy6^{\Delta/\Delta}$ mice (*scale bar*, 60 μm) (*E*) and AC5/6 staining with ciliary marker (acetyl tubulin) and basal body marker (γ-tubulin) in $Adcy6^{f/f}$ tracheal epithelial cells (*scale bar*, 5 μm) (*F*). *G*, hematoxylin/eosin–stained $Adcy6^{f/f}$ and $Adcy6^{\Delta/\Delta}$ tracheal sections (*left panel*; *scale bar*, 300 μm), acetyl tubulin–stained cilia (*middle panel*; *scale bar*, 5 μm), and DIC images (*right panel*; *scale bar*, 2.5 μm) of ciliary tuft in $Adcy6^{f/f}$ and $Adcy6^{\Delta/\Delta}$ mouse tracheal sections. *H*, quantitation of cilia length in $Adcy6^{f/f}$ and $Adcy6^{\Delta/\Delta}$ mouse trachea ($n = 5$ mice/group). Each *dot* represents an average of a single ciliary tuft with 5–10 cilia. *I*, isolated cilia from PBHECs treated with control and AC6 shRNA1 and 2 lentiviral particles and stained with acetyl tubulin (*scale bar*, 1 μm). At *right* are the DIC images of ciliary tuft in PBHEC differentiated on Transwells and treated with control and AC6 shRNA lentiviral particles (*scale bar*, 5 μm). *J*, quantitation of cilia length in PHBECs from Fig. 1*I* (isolated and ciliary tuft combined from $n = 3$ Transwells/group). Each *dot* represents an average of a single ciliary tuft with 5–10 cilia or an average of 5 isolated cilia). Student's *t* test was used for a pair-wise comparison with $P < 0.05$ considered significant. For multiple comparisons one-way ANOVA was used with the *P* value adjusted using Bonferroni's factor. *Con*, control.

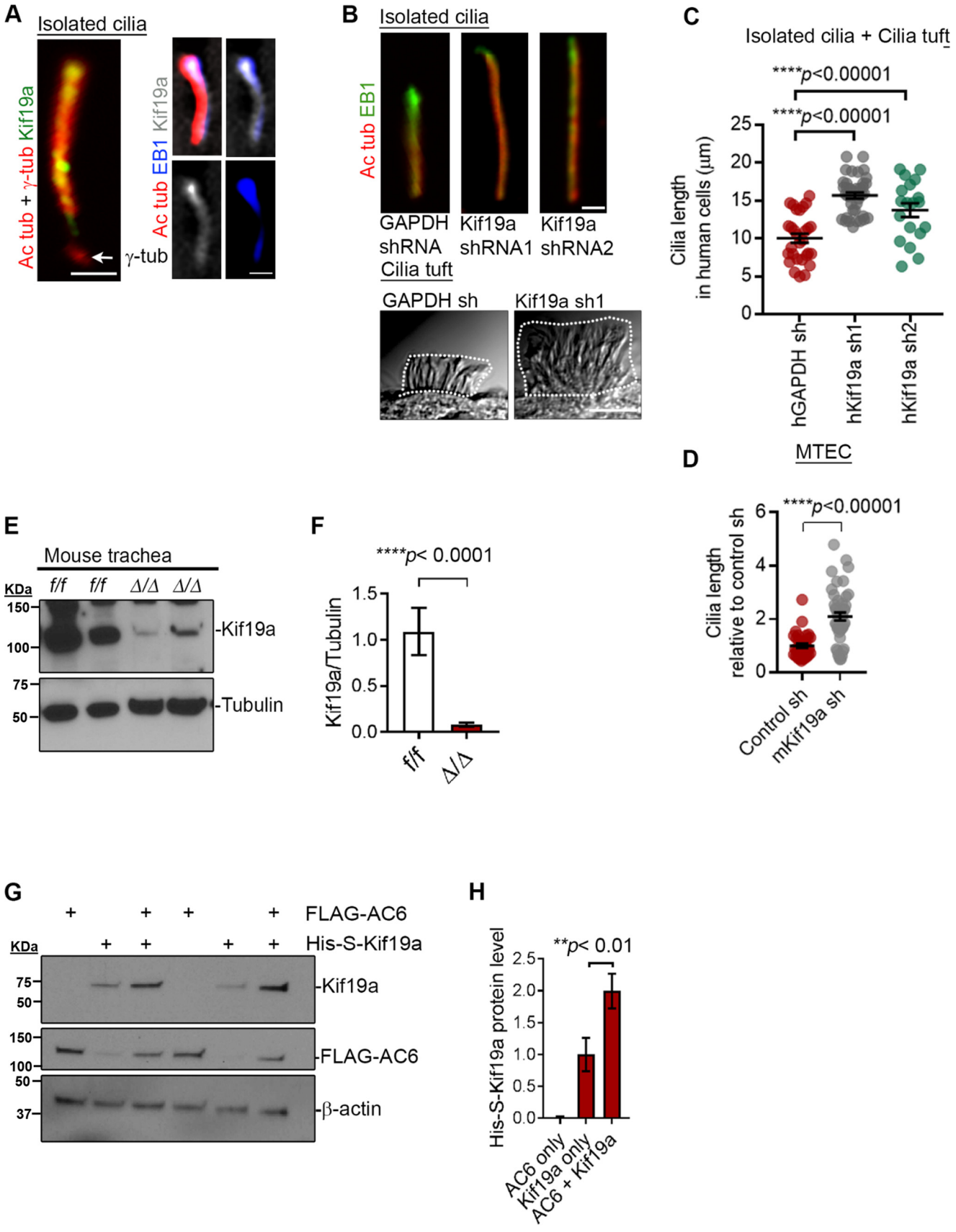
A
Isolated cilia
Ac tub + γ-tub Kif19a
Ac tub EB1 Kif19a
γ-tub
B
Isolated cilia
Ac tub EB1
GAPDH shRNA
Kif19a shRNA1
Kif19a shRNA2
Cilia tuft
GAPDH sh
Kif19a sh1
C
Isolated cilia + Cilia tuft
****p<0.00001
****p<0.00001
Cilia length in human cells (μm)
hGAPDH sh
hKif19a sh1
hKif19a sh2
D
MTEC
****p<0.00001
Cilia length relative to control sh
Control sh
mKif19a sh
E
Mouse trachea
KDa
f/f f/f Δ/Δ Δ/Δ
150
100
75
50
-Kif19a
-Tubulin
F
****p< 0.0001
Kif19a/Tubulin
f/f
Δ/Δ
G
FLAG-AC6
His-S-Kif19a
KDa
75
50
150
100
50
37
-Kif19a
-FLAG-AC6
-β-actin
H
**p< 0.01
His-S-Kif19a protein level
AC6 only
Kif19a only
AC6 + Kif19a

by Cincinnati Children's Hospital Medical Center's Institutional Animal Care and Use Committee.

Chemicals and antibodies

Antibodies in this study included AC5/6 (Santa Cruz), Kif19a (Proteintech), acetyl-tubulin (Sigma), γ-tubulin (Sigma), LC3 (Sigma), β-actin (Sigma), AMPK and mTOR sampler kit (Cell Signaling Technologies), GAPDH (Cell Signaling Technologies), S-protein HRP (EMD Millipore), IFT88 (EMD Millipore), and ubiquitin (CST). AMPK activator 5-aminoimidazole-4-carboxamide ribonucleotide (AICAR), inhibitor compound C (Dorsomorphin), and Torin1 were purchased from Selleck Chemicals (Houston, TX, USA). Autophagy inhibitor chloroquine was obtained from MP Biomedicals (Santa Ana, CA, USA).

Cell transfection

HEK 293 and 16 HBE14o$^-$ cells were obtained from ATCC. HEK 293 and 16 HBE14o$^-$ cells were cultured in DMEM/F-12 and minimal essential medium, respectively, containing 10% FBS and 1% penicillin–streptomycin. Kif19a cDNA isoform 2 was obtained from GE Dharmacon (Lafayette, CO, USA) with a molecular mass coming close to 70 kDa (the molecular mass of the native form of Kif19a is 111 kDa) and inserted into pTriEx vector backbone. pTriEx Kif19a cDNA was transfected by using Lipofectamine 3000 (Thermo Fisher Scientific) according to the manufacturer's protocol. Transfected cells were studied after 48 h. Primary human bronchial epithelial cells were obtained as differentiated on Transwells from two sources: the Cystic Fibrosis Center of the Cincinnati Children's Hospital Medical Center and Charles River Laboratories (Wilmington, MA, USA).

Ready-to-transduce GIPZ lentiviral shRNA particles (mouse and human scrambled AC6 and Kif19a shRNA) were obtained from GE Dharmacon. Primary human bronchial epithelial cells were treated with the 5×10^5 transduction units viral particles for 48 h on the filters (added to the basolateral side) followed by 48 h of recovery and then again treated with 2.5×10^5 transduction units viral particles for 48 h before the experiment. At least two shRNAs were used for AC6 and Kif19a in human cells. For murine cells AC6 and Kif19a shRNAs were used singly or in a combination of two. A 50–60% knockdown efficiency was obtained using these shRNAs.

PHBECs were generated from three donors from the two sources combined. Transduction controls comprised of either nonsilencing lentiviral particles or GAPDH shRNA.

Mouse tracheal epithelial cell culture

Protocol for isolation of tracheal cells was designed with slight modifications from a previously established method (21). Briefly, the trachea were collected in ice-cold Ham's F-12/pen–strep/1× fungizone, and connective, muscular, and vascular tissues were removed manually using forceps. The tracheal tube was opened longitudinally and washed twice in Ham's F-12. Tracheal tissue was incubated in Ham's F-12 with 0.15% Pronase at 4°C and kept upright. Glass-bottomed dishes (Maktek) or plastic culture plates were coated with 50 μg/ml type I rat tail collagen in 0.02 N acetic acid for 18 h at room temperature. The next day, the tissue was transferred into 10 ml of Falcon containing 10 ml of DMEM/F-12 medium with 10% FBS, 1% pen–strep and pipetted up and down several times. Supernatant was collected and spun at 1200 rpm for 10 min. The pellet was resuspended in 200 μl of Ham's F-12/pen–strep containing crude pancreatic DNase I 500 μg/ml, 0.1% BSA and incubated on ice for 5 min. Next, 10 ml of DMEM/F-12 medium is added and spun at 1200 rpm for 10 min. The pellet is resuspended in 3 ml of DMEM medium and kept for 3–4 h in 5% CO_2 at 37°C to remove fibroblasts. Nonadherent cells were collected and centrifuged at 1200 rpm for 5 min at 4°C. The cell pellet was resuspended in mouse tracheal epithelial cell culture medium ((Ham's F-12, 1% penicillin-streptomycin, 5% FBS, 1 × fungizone (Stock 1000 ×), insulin (10 μg/ml), transferrin (5 μg/ml), mEGF (25 ng/ml), bovine pituitary extract (30 μg/ml), cholera toxin (0.1 μg/ml), and retinoic acid (0.5 nM)); the cells were counted and plated in 2D culture or on the costar Transwells.

Cilia-generated flow measurement

Cilia-generated flow measurement in the whole trachea was performed as described previously (22). Briefly, whole trachea were excised from mice and bathed in Leibovitz's L-15 medium containing 10% FBS. Thin tracheal rings were cut under a M165FC stereomicroscope (Leica Biosystems, Wetzlar, Germany) and mounted in 1-mm-spaced slice anchors (Warner Instruments, Hamden, CT, USA). The samples were placed under BX61WI fixed-stage motorized upright microscope (Olympus, Tokyo, Japan). FITC-conjugated beads (0.5 μm) were added to the samples. Bead flow was measured at 32 frames/s. Quantitation of bead velocity was performed as described earlier (22).

Figure 2. AC6 KO mice airway cilia are deficient in ciliary kinesin Kif19a. *A*, isolated cilia from PHBECs immunostained for Kif19a (*green*) and acetyl tubulin (*Ac tub*) + γ-tubulin (*γ-tub*, *red*, *left panel*; *scale bar*, 5 μm) and EB1 (*blue*), Kif19a (*gray*), and acetyl tubulin (*red*, *right panel*; *scale bar*, 5 μm). *B*, *left panel*, isolated cilia from PHBECs treated with GAPDH sh and Kif19a sh1/sh2 (*scale bar*, 2 μm). *Middle panel*, immunostained for ciliary tip marker EB1 (*green*) and acetyl tubulin (*red*). *Right panel*, DIC images of ciliary tuft from PHBECs treated with GAPDH sh and Kif19a sh1/sh2 (*scale bar*, 5 μm). *C*, quantitation of cilia length PHBECs treated with either GAPDH shRNA or Kif19a shRNA lentiviral particles ($n = 3$ separate Transwells). Each *dot* represents an average of a single ciliary tuft with 5–10 cilia or an average of five isolated cilia. *D*, MTECs isolated from WT mice and treated with control shRNA or Kif19a shRNA lentiviral particles ($n = 3$ independent cell preparation). Each *dot* represents an average of five cilia. *E*, Western blotting data probed using Kif19a antibody (*top panel*) demonstrate down-regulation of Kif19a protein expression in *Adcy6*$^{\Delta/\Delta}$ compared with *Adcy6*$^{f/f}$ trachea. Acetyl tubulin (*bottom panel*) was used as a loading marker. *F*, quantitation of Kif19a protein expression in *Adcy6*$^{\Delta/\Delta}$ compared with *Adcy6*$^{f/f}$ trachea from the Western blotting as represented in *E* ($n = 4$ mice/group). *G*, Western blotting probed using S-protein-HRP antibody demonstrates up-regulation of His-S-Kif19a protein expression in 16 HBE14o$^-$ cells with and without overexpression of FLAG-AC6. β-Actin (*bottom panel*) was used as a loading marker. *H*, quantitation of His-S-Kif19a expression in HEK 293 cells ($n = 5$ independent experiments) as represented in the Western blotting in *G*. *Error bars* represent S.E. Student's *t* test was used for a pair-wise comparison with $P < 0.05$ considered significant. For multiple comparisons one-way ANOVA was used with *P* value adjusted using Bonferroni's factor.

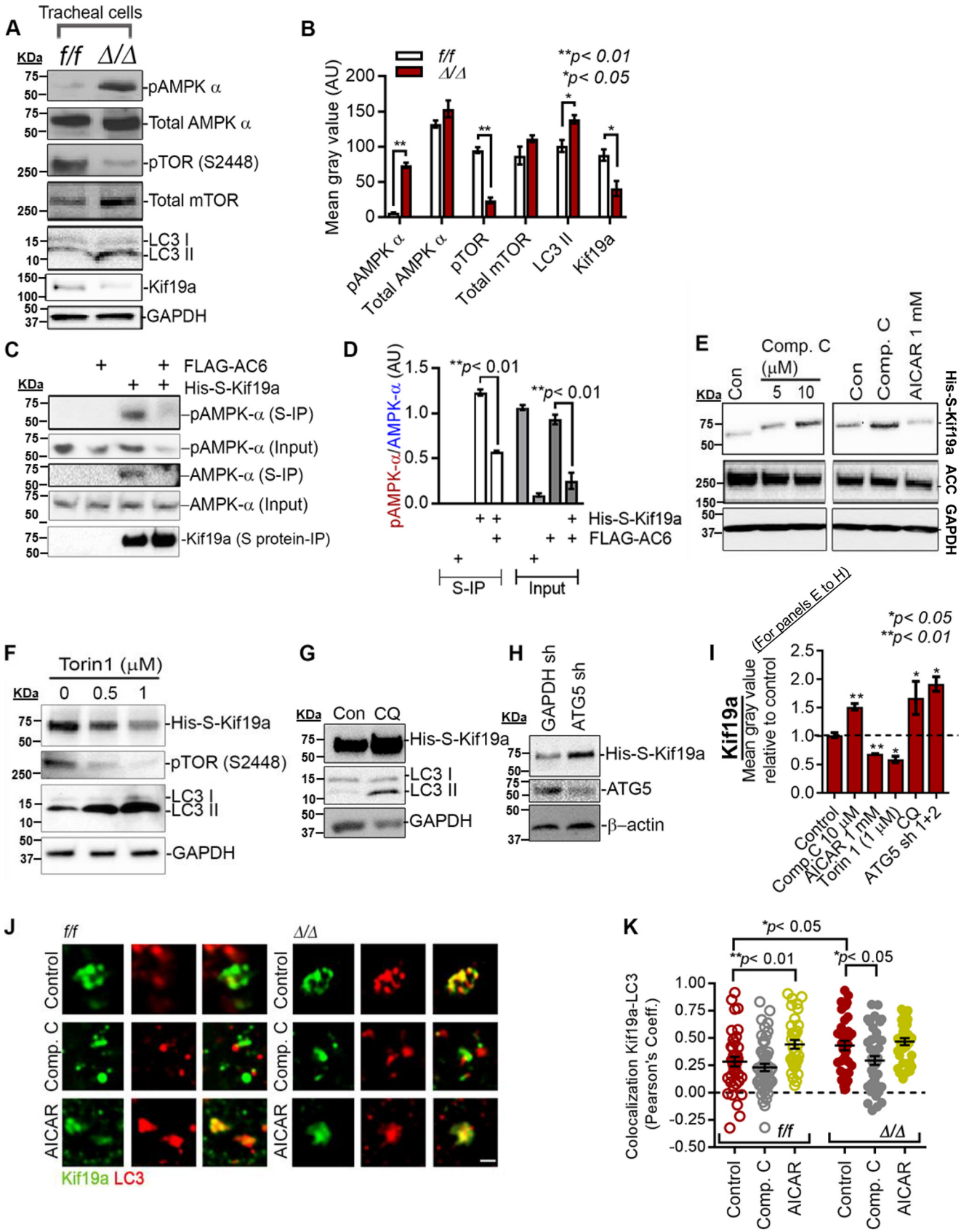
A
Tracheal cells
KDa
f/f
Δ/Δ
75
50
pAMPK α
Total AMPK α
250
pTOR (S2448)
Total mTOR
15
10
LC3 I
LC3 II
150
100
Kif19a
GAPDH
37
B
f/f
Δ/Δ
**p< 0.01
*p< 0.05
Mean gray value (AU)
200
150
100
50
0
pAMPK α
Total AMPK α
pTOR
Total mTOR
LC3 II
Kif19a
C
FLAG-AC6
His-S-Kif19a
pAMPK-α (S-IP)
pAMPK-α (Input)
AMPK-α (S-IP)
AMPK-α (Input)
Kif19a (S protein-IP)
D
pAMPK-α/AMPK-α (AU)
1.5
1.0
0.5
0.0
**p< 0.01
**p< 0.01
His-S-Kif19a
FLAG-AC6
S-IP
Input
E
Comp. C (μM)
5
10
Con
Con
Comp. C
AICAR 1 mM
His-S-Kif19a
ACC
GAPDH
F
Torin1 (μM)
0
0.5
1
His-S-Kif19a
pTOR (S2448)
LC3 I
LC3 II
GAPDH
G
Con
CQ
His-S-Kif19a
LC3 I
LC3 II
GAPDH
H
GAPDH sh
ATG5 sh
His-S-Kif19a
ATG5
β–actin
I
(For panels E to H)
*p< 0.05
**p< 0.01
Kif19a
Mean gray value relative to control
2.5
2.0
1.5
1.0
0.5
0.0
Control
Comp C 10 μM
AICAR 1 mM
Torin 1 (1 μM)
CQ
ATG5 sh 1+2
J
f/f
Δ/Δ
Control
Comp. C
AICAR
Kif19a LC3
K
*p< 0.05
**p< 0.01
*p< 0.05
Colocalization Kif19a-LC3 (Pearson's Coeff.)
1.00
0.75
0.50
0.25
0.00
-0.25
-0.50
f/f
Δ/Δ
Control
Comp. C
AICAR
Control
Comp. C
AICAR

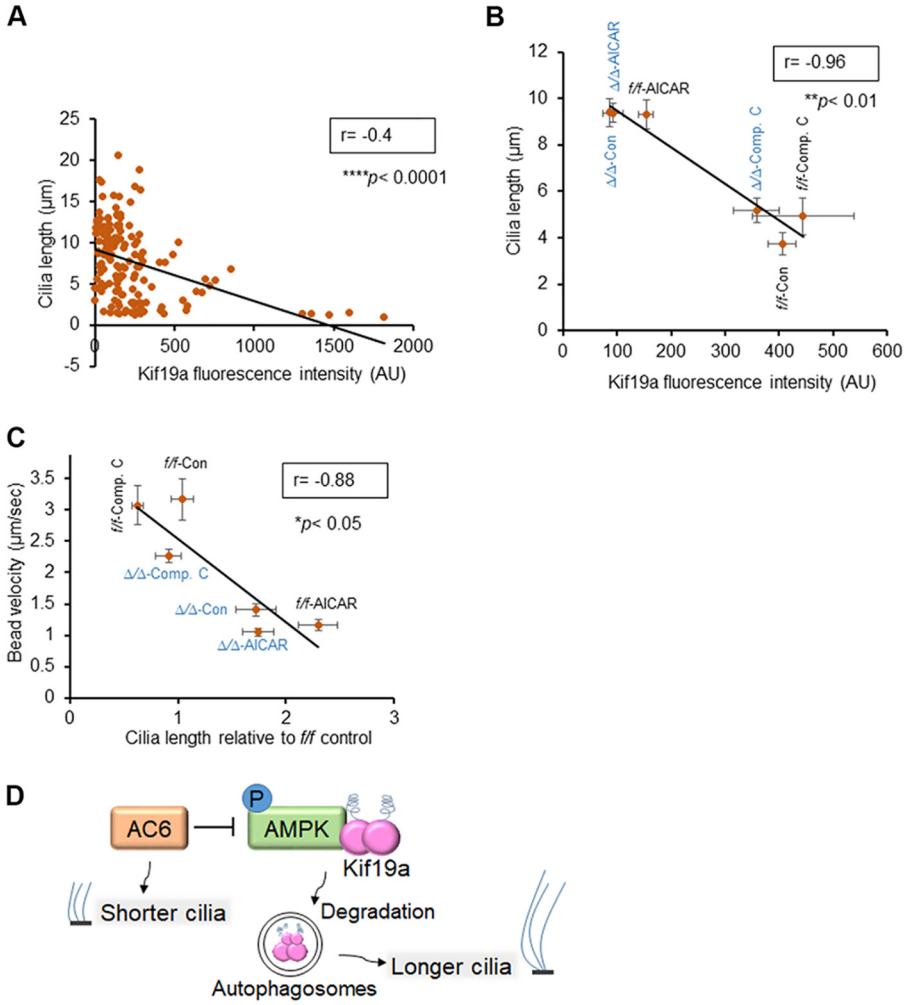

Figure 4. AMPK pathway regulates motile cilia length correlating with altered Kif19a expression. *A*, dot plot to show negative correlation determined using Pearson coefficient (*r*) between ciliary length (based on acetyl tubulin staining) and Kif19a expression (Kif19a-specific immunostaining) in a total of 159 ciliary tufts. *B*, dot plot to show negative correlation determined using Pearson coefficient (*r*) between ciliary length (based on acetyl tubulin staining) and Kif19a expression (Kif19a-specific immunostaining) in $Adcy6^{f/f}$ and $Adcy6^{\Delta/\Delta}$ MTECs on Transwells treated with compound C (5 μM, 24 h) and AICAR (1 mM, 24 h) (n = 23–60 ciliary tufts). *C*, dot plot to show negative correlation determined using Pearson coefficient (*r*) between cilia-generated flow marked by bead velocity and ciliary length (determined in hematoxylin/eosin staining) in $Adcy6^{f/f}$ and $Adcy6^{\Delta/\Delta}$ tracheal rings treated with compound C (10 μM, 4 h) and AICAR, (1 mM, 4 h) (n = 3–5 tracheal rings from 3 mice/group). *D*, model of dynamic regulation of motile cilia length in which AC6 acts a checkpoint for ciliary growth via negative regulation of AMPK activity to prevent autophagic clearance of ciliary depolymerizing kinesin Kif19a. *Error bars* represent S.E.

Cell lysate preparation and coimmunoprecipitation

HEK 293 cells transiently expressing His-S-Kif19a ± FLAG-AC6 were lysed in PBS with 0.2% Triton X-100 containing protease-inhibitor mixture (1 μM aprotonin, 1 μM leupeptin, and 1 mM phenylmethylsulfonyl fluoride). To immunoprecipitate His-S-Kif19a, S-protein–agarose was added to the whole cell lysate and mixed overnight at 4 °C. Proteins immobilized on beads were eluted using 5× sample buffer and subjected to SDS–PAGE and Western blotting. Whole lung cells and MTECs were lysed in radioimmune precipitation assay buffer

Figure 3. AMPK pathway regulates expression of ciliary kinesin Kif19a. *A*, Western blotting of $Adcy6^{\Delta/\Delta}$ and $Adcy6^{f/f}$ whole trachea demonstrates up-regulated AMPK activation (increased P-AMPK α) and autophagy (increased LC3-II expression) with concomitant down-regulation of mTOR pathway (decreased P-TOR). *B*, quantitation of expression levels of various proteins in $Adcy6^{\Delta/\Delta}$ and $Adcy6^{f/f}$ tracheal lysates as represented in *A*. *C*, Western blotting data depicting an interaction between His-S-Kif19a and P-AMPK α and β (and total AMPK α and β) in HEK 293 cells with and without an overexpression of FLAG-AC6 probed using antibodies specific to AMPK subunits. Overexpression of AC6 compromises interaction between Kif19a and AMPK subunits. *D*, quantitation of ratio of expression levels of phospho-AMPK (P-AMPK) to the total AMPK detected in S-protein immunoprecipitation and input as represented in *E*. *E*, Western blot showing protein expression of His-S-Kif19a probed using S-protein-HRP in response to treatment of 16 HBE14o$^-$ cells with AMPK inhibitor (compound C, 5 and 10 μM, 24 h), and activator (AICAR, 1 mM, 24 h). *F–H*, Western blot showing protein expression of His-S-Kif19a probed using S-protein-HRP in response to treatment of 16 HBE14o$^-$ cells with mTOR inhibitor and an autophagy activator Torin1 (0, 0.5 and 1 μM, 2 h) (*F*), autophagy clearance inhibitor CQ (20 μM, 4 h) (*G*), and nonsilencing and ATG5 shRNA lentiviral particles (*H*). *I*, quantitation of His-S-Kif19a protein levels from Western blotting data as represented in *G–J*. *J*, confocal images demonstrate colocalization between Kif19a and autophagosomal marker (LC3) in $Adcy6^{f/f}$ and $Adcy6^{\Delta/\Delta}$ tracheal epithelial cells treated with compound C (5 μM, 24 h) and AICAR (1 mM, 24 h) (*scale bar*, 1.5 μm). *K*, colocalization plot between Kif19a (*green*) and LC3 (*red*) in $Adcy6^{f/f}$ and $Adcy6^{\Delta/\Delta}$ MTECs as represented in *J* (n = 3 independent experiments). Each *dot* represents the average of 3–5 cilia/cell. *Error bars* represent S.E. Student's *t* test was used for a pair-wise comparison and one-way ANOVA with Bonferroni adjustment for multiple comparisons. $P < 0.05$ was considered statistically significant. *Con*, control; *Comp. C*, compound C; IP, immunoprecipitation.

(CST) containing protease inhibitors. Endogenous Kif19a was immunoprecipitated from whole-lung lysate using anti-Kif19a antibody cross-linked to protein A–agarose (0.5 μg of antibody per 10 μl of protein A–conjugated resin by using disuccinimidyl suberate cross-linker). Proteins immobilized on beads were eluted using a low-pH, glycine-based elution buffer containing 0.2% Triton X-100. The samples were incubated for 10 min at 37 °C and subjected to SDS–PAGE and Western blotting.

Immunofluorescence

PHBECs and MTECs were fixed using 3.7% formaldehyde for 15 min at 25 °C. The cells were then washed and permeabilized using PBS with 0.3% Triton X-100 for 30 min at 25 °C. After a brief wash, the cells were blocked with 2% BSA–PBS–Tween-20 for 1 h at 25 °C. The cilia were stained with acetyltubulin antibody (1:1000). Alexa Fluor–conjugated antibodies were used for detection. The images were taken using a confocal microscope (Olympus FV1200). In the immunofluorescence controls, no antibody was added to the samples.

Real-time PCR

RNA was extracted using Qiagen RNeasy mini kit. cDNA was synthesized using SuperScript III reverse transcriptase (Thermo Scientific). Sybr green-based real-time PCR was performed using prevalidated primers for selected murine genes.

Statistics

At least three independent experiments were performed for quantitative measurement. *Error bars* represent S.E. Student's *t* test was used for a pair-wise comparison with two-tailed analysis, and one-way ANOVA was applied for multiple comparisons. The *P* value was adjusted using Bonferroni's correction. A *P* value <0.05 was considered significant.

Data availability

All the data are included in the article.

Acknowledgments—We are grateful to Dr. Gail Pyne-Geithman for editing the manuscript.

Author contributions—K. A. and A. P. N. conceptualization; K. A. formal analysis; K. A. and A. P. N. funding acquisition; K. A. and A. P. N. validation; K. A., J. R. L., N. A. N., B. Z., and A. P. N. investigation; K. A. and A. P. N. methodology; K. A. writing-original draft; B. Z. and A. P. N. resources; A. P. N. supervision; A. P. N. project administration; A. P. N. writing-review and editing.

Funding and additional information—This work was supported by the National Institutes of Health Grants HL147351, DK080834, DK093045, and P30 DK117467 (to A. P. N.), Cystic Fibrosis Foundation grants (to K. A. and A. P. N.), and a Gilead scholarship (to K. A.). The content is solely the responsibility of the authors and does not necessarily represent the official views of the National Institutes of Health.

Conflict of interest—The authors declare that they have no conflicts of interest with the contents of this article.

Abbreviations—The abbreviations used are: AC, adenylate cyclase; KO, knockout; AMPK, AMP-activated kinase; PHBEC, primary human bronchial epithelial cell; MTEC, mouse tracheal epithelial cell; P-, phosphorylated; C, chloroquine; GAPDH, glyceraldehyde-3-phosphate dehydrogenase; HRP, horseradish peroxidase; AICAR, 5-aminoimidazole-4-carboxamide ribonucleotide; DMEM, Dulbecco's modified Eagle's medium; FBS, fetal bovine serum; pen–strep, penicillin–streptomycin; ANOVA, analysis of variance; DIC, differential interference contrast.

References

1. Fliegauf, M., Benzing, T., and Omran, H. (2007) When cilia go bad: cilia defects and ciliopathies. *Nat. Rev. Mol. Cell Biol.* **8,** 880–893 CrossRef Medline
2. Tobin, J. L., and Beales, P. L. (2009) The nonmotile ciliopathies. *Genet. Med.* **11,** 386–402 CrossRef Medline
3. Matsui, H., Randell, S. H., Peretti, S. W., Davis, C. W., and Boucher, R. C. (1998) Coordinated clearance of periciliary liquid and mucus from airway surfaces. *J. Clin. Invest.* **102,** 1125–1131 CrossRef Medline
4. Leopold, P. L., O'Mahony, M. J., Lian, X. J., Tilley, A. E., Harvey, B. G., and Crystal, R. G. (2009) Smoking is associated with shortened airway cilia. *PLoS One* **4,** e8157 CrossRef Medline
5. Hessel, J., Heldrich, J., Fuller, J., Staudt, M. R., Radisch, S., Hollmann, C., Harvey, B. G., Kaner, R. J., Salit, J., Yee-Levin, J., Sridhar, S., Pillai, S., Hilton, H., Wolff, G., Bitter, H., *et al.* (2014) Intraflagellar transport gene expression associated with short cilia in smoking and COPD. *PLoS One* **9,** e85453 CrossRef Medline
6. Niwa, S., Nakajima, K., Miki, H., Minato, Y., Wang, D., and Hirokawa, N. (2012) KIF19A is a microtubule-depolymerizing kinesin for ciliary length control. *Dev. Cell* **23,** 1167–1175 CrossRef Medline
7. Moore, B. S., Stepanchick, A. N., Tewson, P. H., Hartle, C. M., Zhang, J., Quinn, A. M., Hughes, T. E., and Mirshahi, T. (2016) Cilia have high cAMP levels that are inhibited by Sonic Hedgehog–regulated calcium dynamics. *Proc. Natl. Acad. Sci. U.S.A.* **113,** 13069–13074 CrossRef Medline
8. Mick, D. U., Rodrigues, R. B., Leib, R. D., Adams, C. M., Chien, A. S., Gygi, S. P., and Nachury, M. V. (2015) Proteomics of primary cilia by proximity labeling. *Dev. Cell* **35,** 497–512 CrossRef Medline
9. Besschetnova, T. Y., Kolpakova-Hart, E., Guan, Y., Zhou, J., Olsen, B. R., and Shah, J. V. (2010) Identification of signaling pathways regulating primary cilium length and flow-mediated adaptation. *Curr. Biol.* **20,** 182–187 CrossRef Medline
10. Salathe, M. (2007) Regulation of mammalian ciliary beating. *Annu. Rev. Physiol.* **69,** 401–422 CrossRef Medline
11. Mao, S., Shah, A. S., Moninger, T. O., Ostedgaard, L. S., Lu, L., Tang, X. X., Thornell, I. M., Reznikov, L. R., Ernst, S. E., Karp, P. H., Tan, P., Keshavjee, S., Abou Alaiwa, M. H., and Welsh, M. J. (2018) Motile cilia of human airway epithelia contain hedgehog signaling components that mediate noncanonical hedgehog signaling. *Proc. Natl. Acad. Sci. U.S.A.* **115,** 1370–1375 CrossRef Medline
12. Murrow, L., and Debnath, J. (2013) Autophagy as a stress-response and quality-control mechanism: implications for cell injury and human disease. *Annu. Rev. Pathol.* **8,** 105–137 CrossRef Medline
13. Pampliega, O., Orhon, I., Patel, B., Sridhar, S., Díaz-Carretero, A., Beau, I., Codogno, P., Satir, B. H., Satir, P., and Cuervo, A. M. (2013) Functional interaction between autophagy and ciliogenesis. *Nature* **502,** 194–200 CrossRef Medline
14. Kahn, B. B., Alquier, T., Carling, D., and Hardie, D. G. (2005) AMP-activated protein kinase: ancient energy gauge provides clues to modern understanding of metabolism. *Cell Metab.* **1,** 15–25 CrossRef Medline
15. Mihaylova, M. M., and Shaw, R. J. (2011) The AMPK signalling pathway coordinates cell growth, autophagy and metabolism. *Nat. Cell Biol.* **13,** 1016–1023 CrossRef Medline

16. Kim, J., Kundu, M., Viollet, B., and Guan, K. L. (2011) AMPK and mTOR regulate autophagy through direct phosphorylation of Ulk1. *Nat. Cell Biol.* **13,** 132–141 CrossRef Medline
17. Stephan, J. S., Yeh, Y. Y., Ramachandran, V., Deminoff, S. J., and Herman, P. K. (2009) The Tor and PKA signaling pathways independently target the Atg1/Atg13 protein kinase complex to control autophagy. *Proc. Natl. Acad. Sci. U.S.A.* **106,** 17049–17054 CrossRef Medline
18. Varga, V., Helenius, J., Tanaka, K., Hyman, A. A., Tanaka, T. U., and Howard, J. (2006) Yeast kinesin-8 depolymerizes microtubules in a length-dependent manner. *Nat. Cell Biol.* **8,** 957–962 CrossRef Medline
19. Tang, Z., Lin, M. G., Stowe, T. R., Chen, S., Zhu, M., Stearns, T., Franco, B., and Zhong, Q. (2013) Autophagy promotes primary ciliogenesis by removing OFD1 from centriolar satellites. *Nature* **502,** 254–257 CrossRef Medline
20. Lam, H. C., Cloonan, S. M., Bhashyam, A. R., Haspel, J. A., Singh, A., Sathirapongsasuti, J. F., Cervo, M., Yao, H., Chung, A. L., Mizumura, K., An, C. H., Shan, B., Franks, J. M., Haley, K. J., Owen, C. A., *et al.* (2013) Histone deacetylase 6–mediated selective autophagy regulates COPD-associated cilia dysfunction. *J. Clin. Invest.* **123,** 5212–5230 CrossRef Medline
21. You, Y., Richer, E. J., Huang, T., and Brody, S. L. (2002) Growth and differentiation of mouse tracheal epithelial cells: selection of a proliferative population. *Am. J. Physiol. Lung Cell Mol. Physiol.* **283,** L1315–L1321 CrossRef Medline
22. Francis, R., and Lo, C. (2013) *Ex vivo* method for high resolution imaging of cilia motility in rodent airway epithelia. *J. Vis. Exp.* **78,** 50343 CrossRef Medline